

# Soft Matter

Accepted Manuscript



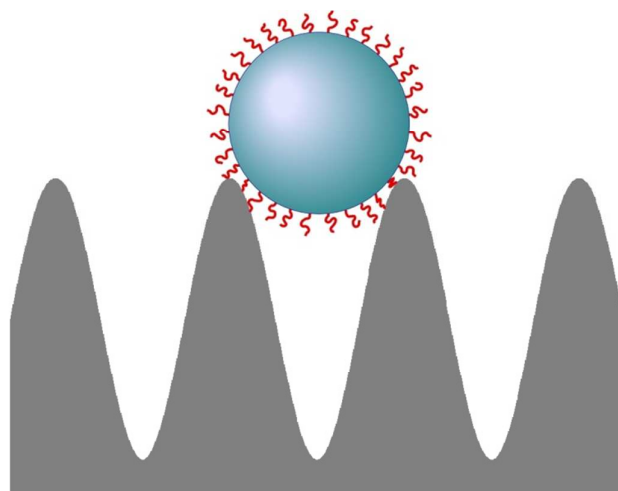
This is an *Accepted Manuscript*, which has been through the Royal Society of Chemistry peer review process and has been accepted for publication.

*Accepted Manuscripts* are published online shortly after acceptance, before technical editing, formatting and proof reading. Using this free service, authors can make their results available to the community, in citable form, before we publish the edited article. We will replace this *Accepted Manuscript* with the edited and formatted *Advance Article* as soon as it is available.

You can find more information about *Accepted Manuscripts* in the [Information for Authors](#).

Please note that technical editing may introduce minor changes to the text and/or graphics, which may alter content. The journal's standard [Terms & Conditions](#) and the [Ethical guidelines](#) still apply. In no event shall the Royal Society of Chemistry be held responsible for any errors or omissions in this *Accepted Manuscript* or any consequences arising from the use of any information it contains.

TOC figure



# Adsorption of “Soft” Spherical Particles onto Sinusoidally-Corrugated Substrates

Phillip K. Schoch and Jan Genzer\*

Department of Chemical & Biomolecular Engineering

North Carolina State University

Raleigh, NC 27695, USA

## Abstract

We utilize a Monte Carlo simulation scheme based on the bond fluctuation model to simulate settlement of "soft" adhesive particles onto sinusoidally-corrugated substrates. Particles are composed of a hard inner core with a "soft" adhesive shell made of surface-grafted polymer chains. These chains adhere to surface lattice sites via pair wise non-specific interactions acting between the substrate and the last two segments of the polymer grafts on the particle. This simulation scheme is aimed at comprehending single particle adsorption behavior to find the highest adhesion energy locations for given test surfaces and elucidate test surfaces that reduce adhesion energy. Parameters in this study are set by the particle, the substrate and an interaction parameter between the two. Particle parameters include core diameter ( $D$ ), grafting density of polymer ( $\sigma$ ) and length of grafted polymer ( $N$ ). Substrate parameters include wavelength ( $\lambda$ ) and amplitude ( $A$ ). Our results show that the wavelength of substrate features plays a significant role in the settlement of single particle systems. At  $\lambda = D/2$  we observe a minimum in the adhesion energy and at  $\lambda = D$  we observe a uniform settlement location of the particles. Increasing  $N$  leads to a reduction in the effectiveness of substrate topography to direct the settlement of individual particles into specific sites on the substrate.

---

\* Corresponding author: Jan\_Genzer@ncsu.edu

## 1. Introduction

The adhesion and organization of particles on materials surfaces is an area of great interest for many technologies ranging from anti-fouling coatings to sensors to sorting polydisperse particles [1-16]. Here we focus on interaction of particles decorated with long-chain flexible hairs whose “sticky” ends govern particle interactions with topographically-corrugated substrates. Examples that resemble systems with similar design include many biological materials, including, microorganisms (*i.e.*, cyprids, zoospores), bacteria, and proteins that interact with substrates. While in some situations adhesion of such particles is favored (*i.e.*, cell growth matrices, particle sorting), in others, (*i.e.*, anti-biofouling coatings), one seeks to avoid the attachment of these particles to or at least reduce their population on the materials surfaces. Many diverse approaches have been proposed to accomplish these goals. Those involve typically either varying the chemical composition or some physical property of the substrate, *i.e.*, modulus, topography. In recent years, most efforts aiming at reducing the adsorption of biofoulers at surfaces have concentrated on utilizing chemistry by generating ethylene-glycol [17,18,22] and charge-containing surfaces [23,24,25]. A less studied, yet equally important, area involves the utilization of engineered substrate topologies in combating the settlement of foulants on surfaces. While a few studies have demonstrated the promise in reducing fouling by utilizing topographically-corrugated surfaces featuring periodic Sharklet patterns [29], hierarchical wrinkles with multiple dimensions [1,30], corrugated periodic structured surfaces [18,25,29,31-35] or even substrates with random topographical protrusions, very little is understood about the mechanisms by which these surfaces work or which morphologies are best suited towards reducing biofouling. Some work has also suggested an attachment point theory used in

association with testing sinusoidal surfaces [29,31,32,36,37]. However this attachment point theory has not been developed into a working model.

In an effort to better understand the role of surface topography in reducing biofouling and to create a predictive tool to design candidate surfaces, we have developed a Monte Carlo computer simulation scheme that aims to replicate the behavior of fouling particles interacting with periodic topographically corrugated substrates. Foulants include a wide set of organisms ranging from bacteria to micro- and macro-foulers, which encompass a size range from hundreds of nanometers to hundreds to (hundreds of) thousands of microns [30]. The interaction energies of these species in terms of energy per contact point on the substrate are not known. Foulants are simulated as hard core spherical particles covered with coarse-grained polymeric “hairs” protruding from their surface. In this work we explore systematically the adsorption of a single “hairy” particle on sinusoidally-corrugated substrates as a function of the properties of the particle, *i.e.*, the particle diameter, grafting density of adhesive hairs, length of hairs, number of adhesive elements per hair, and energy per polymer coarse grained element-to-surface contact, and the characteristics of the underlying substrate, *i.e.*, the frequency and amplitude of the topographical features. In doing so we seek to identify conditions under which the use of *periodic* substrate structures can effectively reduce particle adhesion. Hence, the scenario studied here represents effectively the adhesion of a single organism, *i.e.*, adsorption in low concentration regime. Simultaneous adsorption of multiple particles onto topographically-corrugated substrates, including the effect of particle crowding and inter-particle interaction, will be addressed elsewhere [39].

## 2. Computer model and analysis of data

We employ a Monte Carlo (MC) computer simulation scheme to model the behavior of particles interacting with topographically-corrugated surfaces. These particles adhere via polymeric “hairs” anchored to their surface; the movements of particles and the flexible “hairs” are governed by the bond fluctuation model (BFM) [38]. The substrates, particles and their “hairs” exist in a cubic lattice comprising  $500 \times 500 \times 500$  lattice cells. BFM dictates a set of 108 possible bond vectors allowed in a cubic lattice as shown by the set of moves:  $P(2,0,0) \cup P(2,1,0) \cup P(2,1,1) \cup P(2,2,1) \cup P(3,0,0) \cup P(3,1,0)$  and their permutations and sign inversions of such [38]. All moves in the BFM are selected randomly and attempted with favorable moves tending towards an increase in adhesion energy. To strike a balance between the entire particle moving and each segment of the surface-grafted polymer moving in the lattice, we operate each on different time scales. In this case, within a MC simulation the Monte Carlo steps act as a time parameter. The set of possible moves in this system consist of coarse-grained polymer chain moves and movement of the entire particle. Polymer chains move on a faster time scale than moves of the overall particle thus the move probabilities are balanced as such. While this scenario creates a pseudo-realistic movement, system testing was performed at high number of MC steps to ensure particles were able to reach multiple maxima in their allotted settlement time. There is no preferential direction imposed on the movement of the particles, *i.e.*, no gravitational or other external force effects, as the particles move spontaneously in three-dimensional space. In the results presented, all particles begin from the same spot located above the center of the test substrate. However, we note that the initial position of the particle in the simulation box does not affect the final outcome, as verified by independent runs, in which particles were allowed to start from randomly chosen initial positions above the substrate. Changes to adhesion energy of

the system are handled by the Metropolis decision algorithm where any move that increases the interaction energy between the substrate and the adhesion points on the polymeric grafts is accepted, but any move that causes a decrease in interaction energy is allowed at a probability proportional to  $e^{\Delta E/kT}$ , where  $\Delta E$  is  $E_{\text{adhesion},i} - E_{\text{adhesion},i-1}$  (Note the difference in sign convention as this deals with energy of adhesion which we treat as a positive quantity thus the algorithm seeks to maximize energy of the system). This simulation scheme maintains randomness in the system thus allowing the particle to escape local energy minima. These MC simulations are given an arbitrary amount of time (we use 1,000 steps per polymer coarse grained element) to first equilibrate the surface anchored arms before the particle itself is allowed to move as a whole. Once released the particle moves freely in any direction within the lattice and the simulation ends after a predetermined set of MC steps. The number of MC steps is adjusted to give each segment of the anchored polymer chains and the particle enough time to sample the surfaces many times, on the order of 10,000 per chain segment. It should also be noted that the use of a lattice may result in non-monotonous behavior in our data analysis due to discretization. More details pertaining to the simulation model are presented in Electronic supplementary information.

**Figure 1a** provides the layout of the simulation set up and defines the parameters of the substrates and the particles employed in the simulation. Specifically, the sinusoidal topographies with adjustable amplitude and wavelength, referred to later as feature height and feature width, respectively. Data discussed in this letter include a set of five feature heights and five feature widths, which combined create 25 unique surfaces for each set of particle conditions tested. The particles are defined by their core diameter ( $D$ ), number of repeat segments in the anchor arms ( $N$ ), grafting density of arms on the particle surface ( $\sigma$ ), and the interaction potential acting

between the adhesive arms points (last two segments of the flexible “hair”) and the surface ( $\epsilon$ ). During the MC simulation we track positional data of all particle-anchored arms and the center of mass of the particle as well as the current adhesion energy of the system. Each set of data discussed here represents the compilation and average of 1,000 identical runs for a single particle for each set at a given combination of the simulation parameters.

In addition to evaluating the aforementioned parameters from the MC simulation, we define two new quantities, *i.e.*, relative penetration depth (RPD) and topography match parameter (TMP), which help track the locus of the particles on the topographical surfaces and determine the fidelity with which the particles “replicate” the surface features, respectively. The RPD of the adsorbing particle inside the periodic structures of surface is defined as:

$$\text{RPD} = \frac{z_{\text{lowest particle}} - z_{\text{peak}}}{z_{\text{peak}} - z_{\text{valley}}} \quad (1)$$

In Equation (1)  $z_{\text{lowest particle}}$  and  $z_{\text{peak}}$  represent the  $z$  position of the bottom of the particle and the top of the substrate feature, respectively, as shown in **Figure 1b**. Negative values of “penetration” denote particles that have penetrated the valleys of the substrate. In contrast positive “penetration” values represent particles that lay above the substrate. Penetration = 0 denotes a situation, where the lowest point of the solid portion of the particle (*i.e.*, excluding hairs) is in line with the dashed horizontal line marked in **Figure 1b**. As will be apparent from the subsequent discussion, the “penetration” parameter is helpful in analyzing the relative performance of surfaces in preventing particles from settling in lower substrate locations. While “penetration” characterizes the position of the particle in the  $z$ -direction of the substrate, we define a parameter unique to periodic surfaces, *i.e.*, TMP (*cf.* **Figure 1c**), which characterizes the position of the particle along the horizontal axis:

$$\text{TMP} = \frac{\sum_i^{\text{\#of trials}} x_{\text{COM},i} - x_{\text{valley}}}{\text{\#of trials}} \quad (2)$$

In Equation (2)  $x_{\text{COM}}$  and  $x_{\text{valley}}$  represent the coordinates of the center of mass (COM) and the valley of the sinusoidal profile (*i.e.*, the point of the particle where  $z=z_{\text{valley}}$ ), respectively. Values of TMP approaching 1 represent cases where the particle COM coincides with the peak in the sinusoidal substrate. In contrast TMP values that converge towards 0 denote situations where the COM of the particle moves towards the valley in the sinusoidal substrate. A low TMP value with a corresponding low standard deviation implies highly ordered settlement in the valley position. As will be demonstrated later, the TMP parameter determines how well the substrate drives the particles to adopt discrete and well-defined settlement locations on the surface.

### 3. Results and Discussion

In **Figure 2** we plot the positions of the center of mass of the largest particles ( $D=20$ ) having the shortest length of the polymeric hair ( $N=3$ ) and grafting density ( $\sigma=0.04$ ) at the intermediate adhesion energy studied ( $\epsilon=1$  kT). The data in **Figure 2** demonstrate visually the dramatic differences in particle settlement as a function of the periodicity (*i.e.*, feature width) and the amplitude (*i.e.*, feature height) of the substrate. In **Figure 3** we plot the values of the RPD, TMP and adhesion energy (along with the standard deviation for the latter two quantities) as a function of the feature width for various values of the feature amplitude. For substrates that possess the largest feature width, the particles settle on lower portions of the substrate (*i.e.*, valleys) and are somewhat spread out, particularly at substrates with lower feature heights. In the small wavelength case, the particles settle relatively uniformly across the substrate.

Substrates, whose feature width matches the diameter of the particles, perform glaringly differently. Specifically, the particles settling on such substrates are allowed to reside only in discrete locations defined by the valleys of the topography. Thus the total number of particles settled is the lowest when the feature width of substrates with periodic topographies featuring sinusoidal profile matches the size of the adsorbing particles because the particles are allowed to reside only in very specific places on the substrate (relative to situations where the particle size and the substrate features do not match). Having established the essential attributes of the system set up and the effect of the substrate periodicity and amplitude on particle population on the substrate, we provide below more detailed account of the effect of the various system parameters that govern the observed phenomenon.

In **Figure 4** we plot the values of the RPD, TMP, and adhesion energy as a function of the feature width for various combinations of  $D$ ,  $N$ ,  $\sigma$ , and  $\epsilon$ . For clarity we only present data pertaining to the adsorption on surfaces that possess low (10, open symbols) and high (80, closed symbols) amplitude. The left column in **Figure 4** denotes situations where  $N=3$ ,  $\sigma=0.04$ , and  $\epsilon=1$  kT and  $D$  varies between 10 (black circles) and 40 (red squares). As expected, larger particles are excluded from penetrating deeper until the feature width of the substrate becomes very large. Also noticeable is the point where the particles first begin to penetrate the substrate features. This occurs when the substrate feature width matches approximately the diameter of the particles, implying that the penetration is highly dependent on the spatial relationship of the size of the particle vs. the size of the spacing between the substrate features. The critical role of the substrate feature width appears again in the TMP dependence on the substrate “wavelength”. Here the value of the TMP and its standard deviation reach a minimum at feature widths corresponding to the diameter of the particle. The values of the TMP also indicate that under

these conditions the particles are both valley-centered and highly ordered in their settlement, although they are still too large to penetrate deep into the substrate.

Having discussed the effect of the particle size, we now turn to exploring the role of the length of the flexible hair on particle adsorption. In the second column from the left in **Figure 4** we plot RPD, TMP, and adhesion energy as a function of the feature width for  $D=20$ ,  $\sigma=0.04$ , and  $\varepsilon=1$  kT and  $N$  equal to 3 (black circles) and 10 (red squares). The RPD data for the short arms reveal that the particles enter the surface structure just above the diameter of the particle whereas the particles with the longer arms are sterically hindered in their penetration due to their bulky arms. The short-armed particles settle discretely on the surface based on the TMP data with high level of ordering. However, the long-armed particles “ignore” the substrate topography to a large degree and settle equally everywhere on the surface. This result implies that the substrate topography is effective in controlling particle settlement only in situations where the particles possess flexible elements whose size is much smaller than their radii; *i.e.*, substrate topographies are ineffective in controlling particle settlement in situations involving particles whose flexible arms are on the order of or longer than the radii of the settling particles.

The grafting density of the flexible arms of the particles’ surfaces also affects particle settlement on the topographically-corrugated substrates. In the second column from the right in **Figure 4** we present RPD, TMP, and adhesion energy as a function of the feature width for  $D=10$ ,  $N=3$ , and  $\varepsilon=1$  kT and  $\sigma$  equal to 0.04 (black circles) and 0.16 (red squares). The RPD data characterize the effect of the density of flexible arms on increasing the chain stiffness as the effective radius of the particle increases causing the particles to penetrate the substrate much more gradually at high grafting density. As expected, relative to the low  $\sigma$  case, particles with high grafting density hairs exhibit much higher adhesion energies due to more adhesive points

acting between the particle and the substrate. The TMP varies only slightly in behavior for the two cases. Also of note is the peak in the adhesion energy plot and its standard deviation; it occurs at roughly two times the particle diameter and may be a case of the particle fitting well into the base of the valley and finding a maximal contact area.

Finally we discuss the role of the adhesion energy on particle adsorption. In the right column in **Figure 4** we present RPD, TMP, and adhesion energy as a function of the feature width for  $D=20$ ,  $N=3$ , and  $\sigma=0.04$  and  $\varepsilon$  equal to 0.5 (black circles) and 2 kT (red squares). This situation is akin to changing the chemistry of the substrate or that of the adhesive ends of the flexible “hairs” attached to the particle surface. Predictably, varying  $\varepsilon$  does not affect the penetration data appreciably as those depend primarily on spatial factors discussed earlier. The TMP, however, is affected much more noticeably as it not only depends on spatial factors, but energetic as well. The case of  $\varepsilon=2$  kT exhibits tight binding of the particle to the substrate at the most favorable positions leading to lower minima in both the TMP and its standard deviation. In addition, as expected, the  $\varepsilon=2$  kT case leads to higher overall adhesion energies (and greater variations) relative to  $\varepsilon=0.5$  kT situations. This data point out that more organized settlement of particles on corrugated substrates can be achieved by increasing the attraction of the particle to the substrate surface. This finding can be beneficial in a variety of fields including particle sorting using controlled adsorption to substrates.

#### 4. Conclusion

We have discussed the settlement of single particles with anchored flexible arms on substrates with periodically-corrugated topologies featuring sinusoidal shapes. We have demonstrated that the adsorption in these situations is governed by the complex interplay between the

characteristics of the substrate (*i.e.*, periodicity and amplitude) and the properties of the particles (*i.e.*, particle size, length and grafting density of the flexible spacers, and the affinity of the adsorptive end-segments of the flexible arms towards the surface). The major conclusion is that substrates featuring *periodic topographical corrugations* whose dimensions are commensurate with the sizes of the adsorbing particles may offer an avenue towards generating *effective passive barriers* for minimizing particle settlement. In the current publication we only tested particle settlement on surfaces featuring sinusoidal periodic topographies. These results are thus directly applicable to providing additional insight into the studies of de Nys et al. [31,32] who invoked the attachment point theory to interpret their biofouling data. The next obvious step is to extend the current study to situations involving adsorption of particles with different sizes and shapes on surfaces featuring non-sinusoidal periodic topographies [39]. Work towards this goal is currently in progress and will be reported in future publications.

### **Acknowledgement**

This work was supported by the Office of Naval Research under Grant No. N000141210642.

## References

1. K. Efimenko, M. Rackaitis, E. Manias, A. Vaziri, L. Mahadevan, J. Genzer. Nested self-similar wrinkling patterns in skins. *Nature Materials*, 2005, **4**, 293-297.
2. C.J. Wohl, M.A. Belcher, L. Chen, J.W. Connell. Laser ablative patterning of copoly(imide siloxane)s generating superhydrophobic surfaces. *Langmuir*, 2010, **26**, 11469-11478.
3. R. Di Mundo, M. Nardulli, A. Milella, P. Favia, R. d'Agostino, R. Gristina. Cell adhesion on nanotextured slippery superhydrophobic substrates. *Langmuir*, 2011, **27**, 4914-4921.
4. Z. Zhang, S. Chen, S. Jiang. Dual-functional biomimetic materials: Nonfouling poly(carboxybetaine) with active functional groups for protein immobilization. *Biomacromolecules*, 2006, **7**, 3311-3315.
5. M. Mrksich. A surface chemistry approach to studying cell adhesion. *Chemical Society Reviews*, 2000, **29**, 267-273.
6. Y. Shao, J. Fu. Integrated Micro/Nanoengineered functional biomaterials for cell mechanics and mechanobiology: A materials perspective. *Advanced Materials*, 2014, **26**, 1494-1533.
7. P. Tseng, D. Di Carlo. Substrates with patterned extracellular matrix and subcellular stiffness gradients reveal local biomechanical responses. *Advanced Materials*, 2014, **26**, 1242-1247.
8. X. Yao, R. Peng, J. Ding. Cell-material interactions revealed via material techniques of surface patterning. *Advanced Materials*, 2013, **25**, 5257-5286.
9. A. Marino, G. Ciofani, C. Filippeschi, M. Pellegrino, M. Pellegrini, P. Orsini, M. Pasqualleti, V. Mattoli, B. Mazzolai. Two-photon polymerization of sub-micrometric patterned surfaces: Investigation of cell-substrate interactions and improved differentiation of neuron-like cells. *ACS Applied Materials & Interfaces*, 2013, **5**, 13012-13021.
10. N.M. Sangeetha, C. Blanck, T.T.T. Nguyen, C. Contal, P.J. Size-selective 2D ordering of gold nanoparticles using surface topography of self-assembled diamide template. *ACS Nano*, 2012, **6**, 8498-8507.
11. W. Bae, H.N. Kim, D. Kim, S. Park, H.E. Jeong, K. Suh. 25th anniversary article: Scalable multiscale patterned structures inspired by nature: The role of hierarchy. *Advanced Materials*, 2014, **26**, 675-700.

12. M.E. Kolewe, H. Park, C. Gray, X. Ye, R. Langer, L.E. Freed. 3D structural patterns in scalable, elastomeric scaffolds guide engineered tissue architecture. *Advanced Materials*, 2013, **25**, 4459-4465.
13. A. Agarwal, Y. Farouz, A.P. Nesmith, L.F. Deravi, M.L. McCain, K.K. Parker. Micropatterning alginate substrates for in vitro cardiovascular muscle on a chip. *Advanced Functional Materials*, 2013, **23**, 3738-3746.
14. C. Hanske, M.B. Mueller, V. Bieber, M. Tebbe, S. Jessl, A. Wittemann, A. Fery. The role of substrate wettability in nanoparticle transfer from wrinkled elastomers: Fundamentals and application toward hierarchical patterning. *Langmuir*, 2012, **28**, 16745-16750.
15. K.E. Snell, N. Stephant, R.B. Pansu, J. Audibert, F. Lagugne-Labarthe, E. Ishow. Nanoparticle organization through photoinduced bulk mass transfer. *Langmuir*, 2014, **30**, 2926-2935.
16. M.K. Driscoll, X. Sun, C. Guven, J.T. Fourkas, W. Losert. Cellular contact guidance through dynamic sensing of nanotopography. *ACS Nano*, 2014, **8**, 3546-3555.
17. S. Krishnan, C.J. Weinman, C.K. Ober. Advances in polymers for anti-biofouling surfaces. *Journal of Materials Chemistry*, 2008, **18**, 3405-3413.
18. C.M. Grozea, G.C. Walker. Approaches in designing non-toxic polymer surfaces to deter marine biofouling. *Soft Matter*, 2009, **5**, 4088-4100.
19. R. Chapman, E. Ostuni, M. Liang, G. Meluleni, E. Kim, L. Yan, G. Pier, H.S. Warren, G.M. Whitesides. Polymeric thin films that resist the adsorption of proteins and the adhesion of bacteria. *Langmuir*, 2001, **17**, 1225-1233.
20. H. Therien-Aubin, L. Chen, C.K. Ober. Fouling-resistant polymer brush coatings. *Polymer*, 2011, **52**, 5419-5425.
21. G. Gunkel, M. Weinhart, T. Becherer, R. Haag, T.W.S. Huck. Effect of polymer brush architecture on antibiofouling properties. *Biomacromolecules*, 2011, **12**, 4169-4172.
22. M.D. Dimitriou, Z. Zhou, H. Yoo, K.L. Killips, J.A. Finlay, G. Cone, H.S. Sundaram, N.A. Lynd, K.P. Barteau, L.M. Campos, D.A. Fischer, M.E. Callow, J.A. Callow, C.K. Ober, C.J. Hawker, E.J. Kramer. A general approach to controlling the surface composition of poly(ethylene oxide)-based block copolymers for antifouling coatings. *Langmuir*, 2011, **27**, 13762-13772.
23. Z. Zhang, T. Chao, S. Chen, S. Jiang. Superlow fouling sulfobetaine and carboxybetaine polymers on glass slides. *Langmuir*, 2006, **22**, 10072-10077.

24. Z. Zhang, J.A. Finlay, L. Wang, Y. Gao, J.A. Callow, M.E. Callow, S. Jiang. Polysulfobetaine-grafted surfaces as environmentally benign ultralow fouling marine coatings. *Langmuir*, 2009, **25**, 13516-13521.
25. G. Li, H. Xue, C. Gao, F. Zhang, S. Jiang. Nonfouling polyampholytes from an ion-pair comonomer with biomimetic adhesive groups. *Macromolecules*, 2010, **43**, 14-16.
26. K. Koch, B. Bhushan, Y.C. Jung, W. Barthlott. Fabrication of artificial lotus leaves and significance of hierarchical structure for superhydrophobicity and low adhesion. *Soft Matter*, 2009, **5**, 1386-1393.
27. L. Feng, S. Li, Y. Li, H. Li, L. Zhang, J. Zhai, Y. Song, B. Liu, L. Kiang, S. Zhu, D. Super-hydrophobic surfaces: From natural to artificial. *Advanced Materials*, 2002, **14**, 1857-1860.
28. M. Sun, C. Luo, L. Xu, H. Ji, Q. Ouyang, D. Yu, Y. Chen. Artificial lotus leaf by nanocasting. *Langmuir*, 2005, **21**, 8978-8981.
29. K. Berntsson, H. Andreasson, P. Jonsson, L. Larsson, K. Ring, S. Petronis, P. Gatenholm,. Reduction of barnacle recruitment on micro-textured surfaces: Analysis of effective topographic characteristics and evaluation of skin friction. *Biofouling*, 2000, **16**, 245-261.
30. K. Efimenko, J. Finlay, M.E. Callow, J.A. Callow, J. Genzer. Development and testing of hierarchically wrinkled coatings for marine antifouling. *ACS Applied Materials & Interfaces*, 2009, **1**, 1031-1040.
31. N. Aldred, A. Scardino, A. Cavaco, R. de Nys, A.S. Clare. Attachment strength is a key factor in the selection of surfaces by barnacle cyprids (*Balanus amphitrite*) during settlement. *Biofouling*, 2010, **26**, 287-299.
32. A. Scardino, E. Harvey, R. De Nys. Testing attachment point theory: Diatom attachment on microtextured polyimide biomimics. *Biofouling*, 2006, **22**, 55-60.
33. R. Vasudevan, A.J. Kennedy, M. Merritt, F.H. Crocker, R.H. Baney. Microscale patterned surfaces reduce bacterial fouling-microscopic and theoretical analysis. *Colloids and Surfaces B: Biointerfaces*, 2014, **117**, 225-232.
34. D. Perera-Costa, J.M. Bruque, M. Gonzalez-Martin, A.C. Gomez-Garcia, V. Vadiello-Rodriguez. Studying the influence of surface topography on bacterial adhesion using spatially organized microtopographic surface patterns. *Langmuir*, 2014, **30**, 4633-4641.
35. A. Grinthal, J. Aizenberg. Mobile interfaces: Liquids as a perfect structural material for multifunctional, antifouling surfaces. *Chemistry of Materials*, 2014, **26**, 698-708.

36. C. Guegan, J. Garderes, G. Le Pennec, F. Gaillard, F. Fay, I. Linossier, J.M. Henry, M.N. Bellon Fontaine, K. Vallee Rehal. Alteration of bacterial adhesion induced by the substrate stiffness. *Colloids and Surfaces B: Biointerfaces*, 2014, **114**, 193-200.
37. J.T. Decker, C.M. Kirschner, C.J. Long, J.A. Finlay, M.E. Callow, J.A. Callow, A.B. Brennan. Engineered antifouling microtopographies: An energetic model that predicts cell attachment. *Langmuir*, 2013, **29**, 13023-13030.
38. I. Carmesin, K. Kremer. The bond fluctuation method - a new effective algorithm for the dynamics of polymers in all spatial dimensions. *Macromolecules*, 1988, **21**, 2819-2823.
39. P.K. Schoch, J. Genzer. Adsorption of multiple spherical particles onto sinusoidally-corrugated substrates, *Langmuir*, 2014, in press, DOI: 10.1021/la502026g.

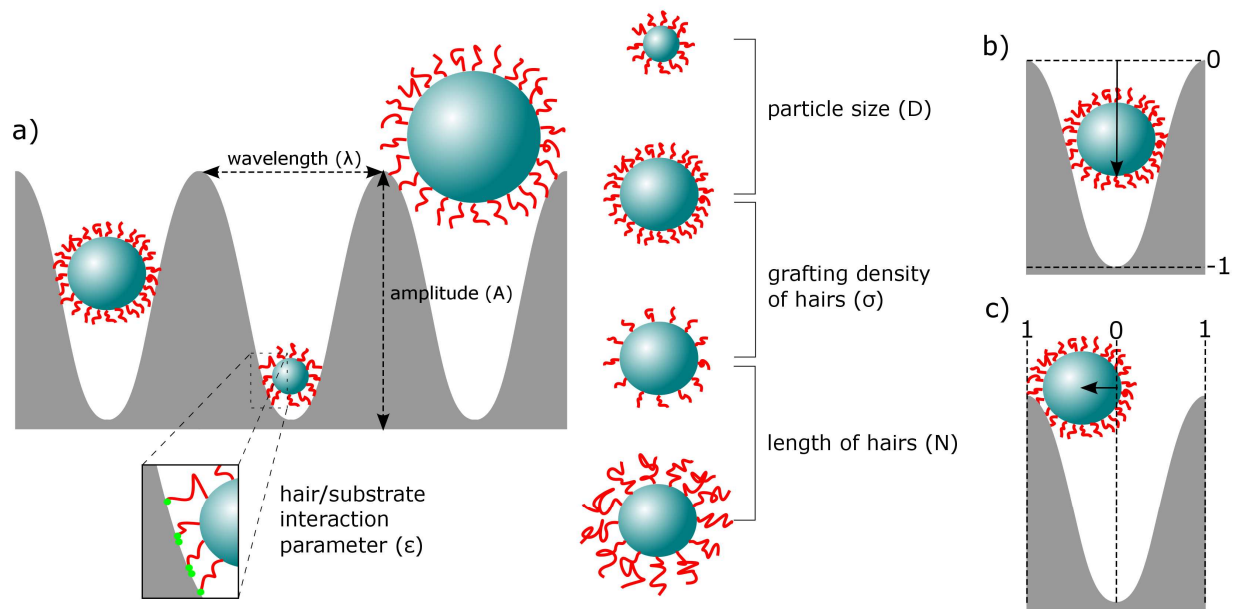


**Figure 1.** a) Simulation setup depicting adhesion of particles with coarse grained polymer hairs on sinusoidally-corrugated substrates. b) Relative penetration depth (RPD), a ratio of particle depth inside of substrate feature to height of given surface feature. c) Topography match parameter (TMP), a factor of particle localization relative to valley and peak locations on periodic substrates.

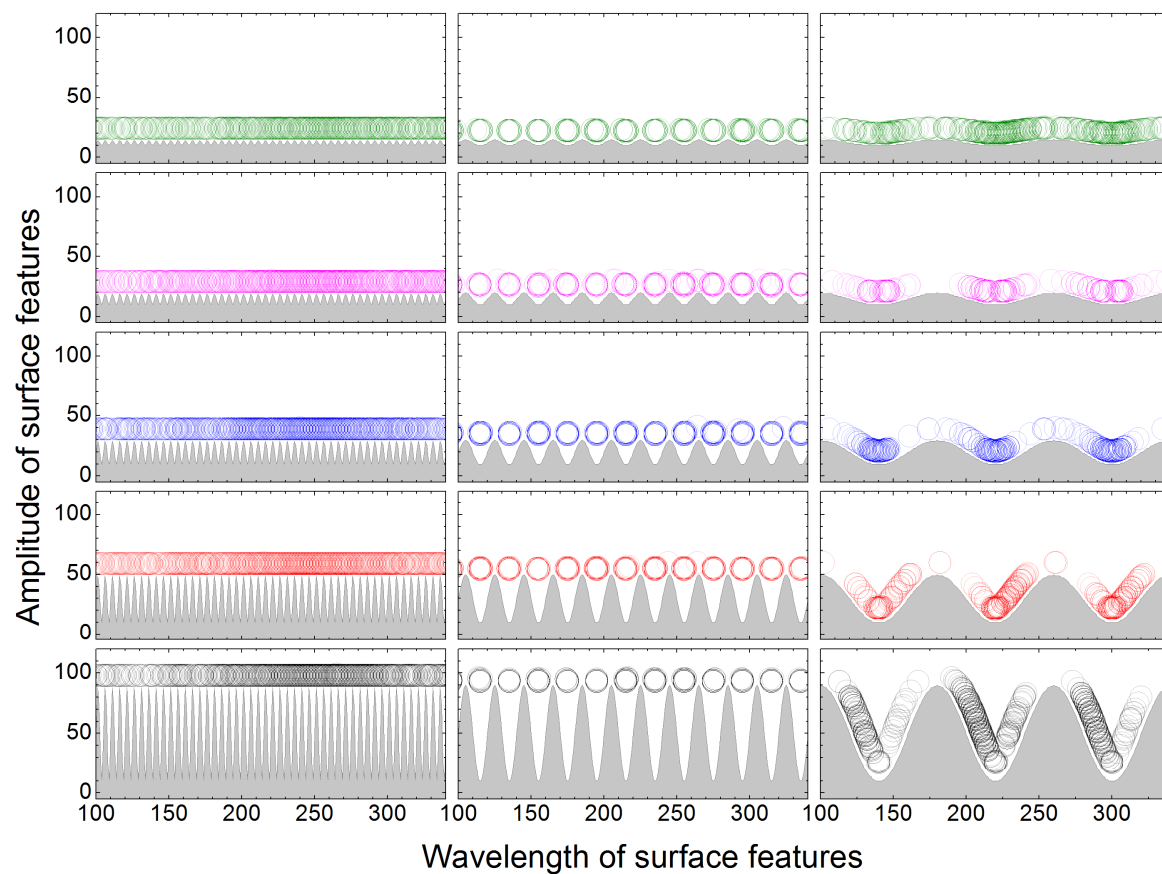


**Figure 2.** Positions of the center of mass (COM) for particles having  $D=20$ ,  $N=3$ ,  $\sigma=0.04$  and  $\epsilon=1$  kT adsorbing on substrates featuring sinusoidal corrugations featuring five different amplitudes and three different feature widths. The amplitudes are equal to (from the top to the bottom panel): 5 (green), 10 (magenta), 20 (blue), 40 (red), and 80 (black). The feature widths displayed are equal to: 5 (left column), 20 (middle column), and 80 (right column). Plotted circles represent core diameter of settled particles, polymer arms not shown.

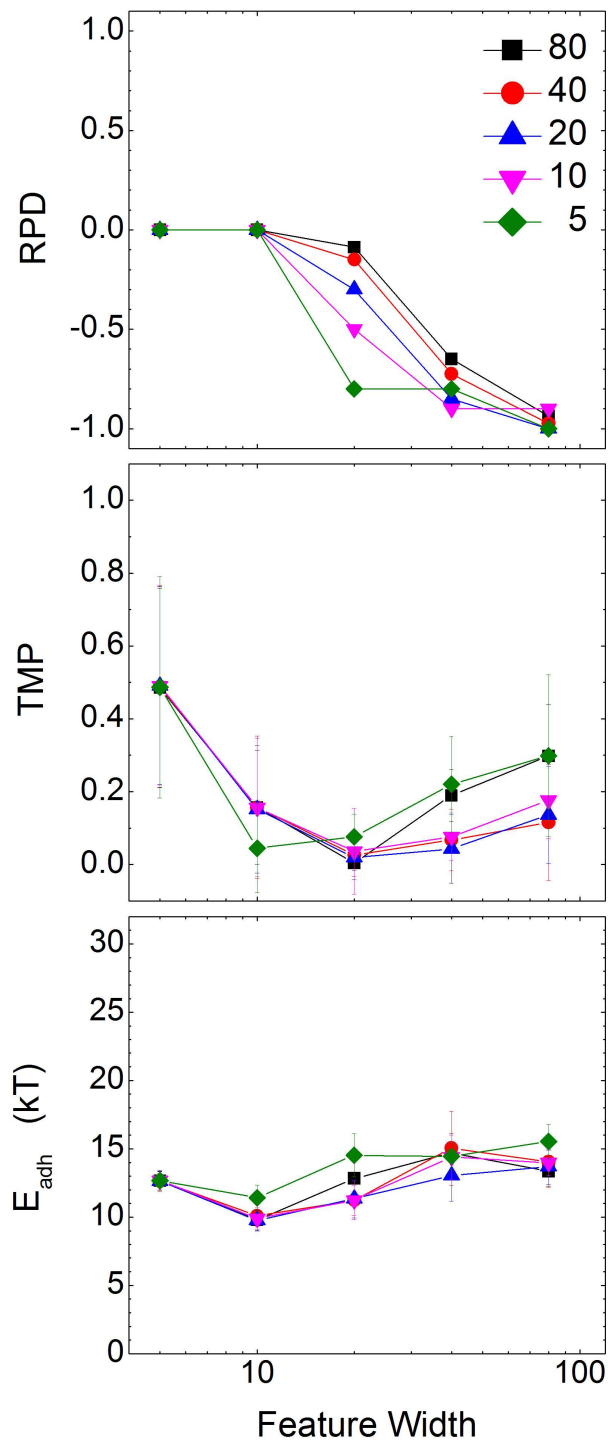


**Figure 3.** Relative penetration depth (RPD), topography match parameter (TMP), and adhesion energy ( $E_{\text{adh}}$ ) as a function of the feature width for particles whose parameters are depicted in Figure 2 adsorbing onto substrates with a sinusoidal topographies having amplitudes equal to: 5 (green diamonds), 10 (magenta down-triangles), 20 (blue up-triangles), 40 (red circles), and 80 (black squares).

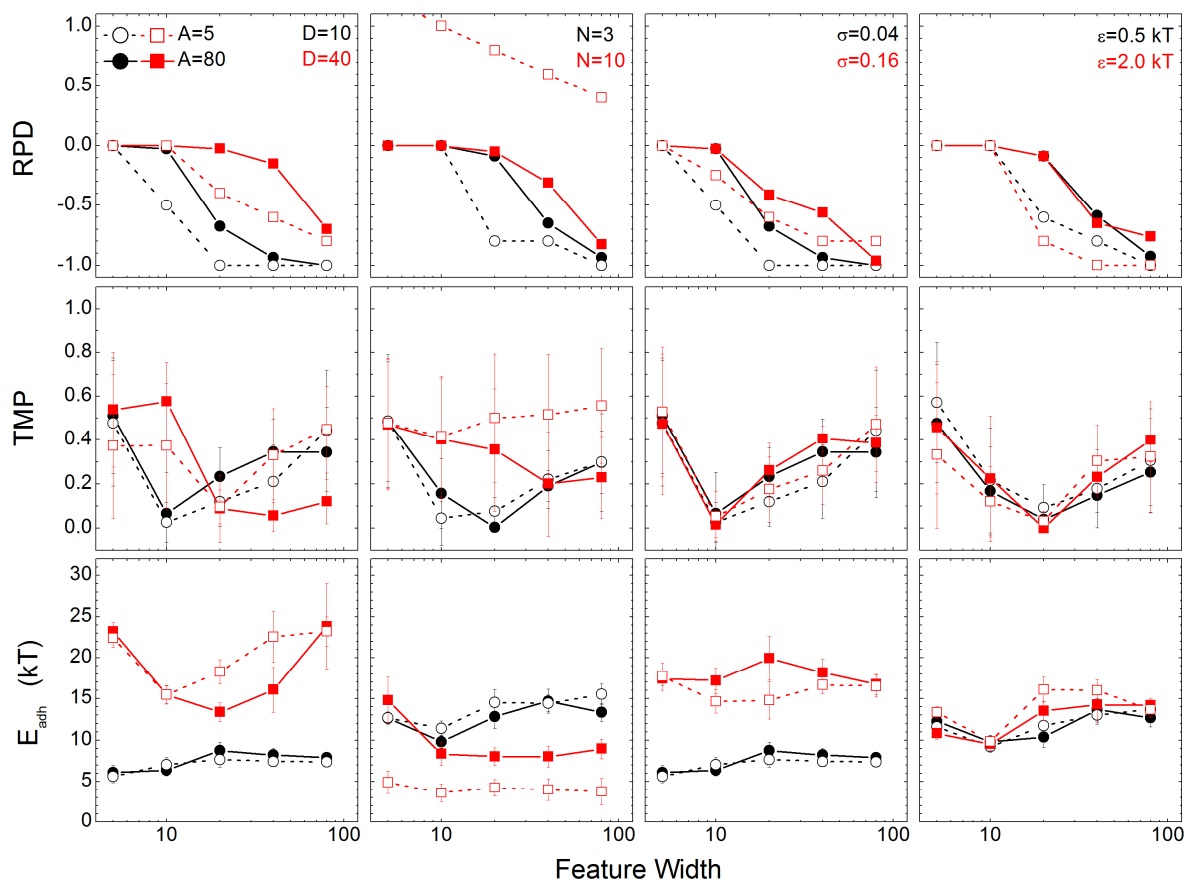


**Figure 4.** Relative penetration depth (RPD, top row), topography match parameter (TMP, middle row), and adhesion energy ( $E_{adh}$ , bottom row) as a function of the feature width for particles adsorbing onto substrates with a sinusoidal topographies having amplitudes equal to 5 (open symbols) and 80 (closed symbols). The black and red symbols represent two cases in which one system parameter was varied, *i.e.*, particle diameter ( $D$ , left column), length of polymer hair ( $N$ , second column from left), grafting density of hair ( $\sigma$ , second column from right), and adhesion energy ( $\epsilon$ , right column).